SCIENTIFIC REPORTS

OPEN

SUBJECT AREAS:
MATERIALS SCIENCE
NANOTECHNOLOGY
CHEMISTRY
METHODS

Received
11 April 2012

Accepted
23 May 2012

Published
12 June 2012

Correspondence and requests for materials should be addressed to H.J.F. (fanhj@ntu.edu.sg)

* These authors contributed equally to this work.

Homogeneous Photosensitization of Complex TiO_2 Nanostructures for Efficient Solar Energy Conversion

Jingshan Luo[1]*, Siva Krishna Karuturi[2]*, Lijun Liu[2], Liap Tat Su[2], Alfred Iing Yoong Tok[2] & Hong Jin Fan[1]

[1]Division of Physics and Applied Physics, School of Physical and Mathematical Sciences, Nanyang Technological University, 637371 Singapore, [2]School of Materials Science and Engineering, Nanyang Technological University, 639798 Singapore.

TiO_2 nanostructures-based photoelectrochemical (PEC) cells are under worldwide attentions as the method to generate clean energy. For these devices, narrow-bandgap semiconductor photosensitizers such as CdS and CdSe are commonly used to couple with TiO_2 in order to harvest the visible sunlight and to enhance the conversion efficiency. Conventional methods for depositing the photosensitizers on TiO_2 such as dip coating, electrochemical deposition and chemical-vapor-deposition suffer from poor control in thickness and uniformity, and correspond to low photocurrent levels. Here we demonstrate a new method based on atomic layer deposition and ion exchange reaction (ALDIER) to achieve a highly controllable and homogeneous coating of sensitizer particles on arbitrary TiO_2 substrates. PEC tests made to CdSe-sensitized TiO_2 inverse opal photoanodes result in a drastically improved photocurrent level, up to ~15.7 mA/cm^2 at zero bias (vs Ag/AgCl), more than double that by conventional techniques such as successive ionic layer adsorption and reaction.

Ever since the seminal paper of photoelectrolysis of water by Fujishima and Honda[1], TiO_2 has received wide attentions in photocatalysts, water splitting and solar cells due to its high photoactivity, low cost and excellent chemical stability[2-5]. The limiting factor for TiO_2 is the large band gap (~3.2 eV), which defines its light absorption only in the UV range. During the past three decades, tremendous efforts have been put to enhance the visible light harvesting ability of TiO_2[6]. Heterogeneous structures have been proposed to couple TiO_2 with materials exhibiting visible light harvesting ability, and the first trial was done by Serpone *et al.* to couple TiO_2 with CdS which showed a significant improvement[7]. Later on Graetzel made a significant breakthrough in sensitizing TiO_2 with dye molecules, viz., the dye-sensitized TiO_2 photoanode[4]. Following the invention of Graetzel cell, quantum dot sensitized solar cells (QDSSC) quickly catch up following the mature quantum dot synthesis protocol developed by Peng and Alivisatos[8,9]. The key development of QDSSC was made by Kamat in 2005, with the pre-synthesized CdSe nanocrystals linked to TiO_2 thin films by organic molecules[10]. Since then various methods of sensitization have been developed, and they can be summarized into two main categories: assembly of pre-synthesized QDs and direct growth[11,12]. Pre-synthesis provides the feasibility of facile control in the size, size distribution and morphology. However, the charge transfer would be retarded by the surface functional molecules. Also the loading of the sensitizer prepared by this method is usually low. Direct growth allows both a compact contact of the sensitizer with TiO_2, and the ease of increasing the loading of the sensitizer. A diverse range of methods are reported for the direct coating of the sensitizing materials, such as chemical bath deposition[13,14], successive ionic layer adsorption and reaction (SILAR)[15-17], electrochemical deposition[18], chemical vapour deposition[19] and electrophoretic deposition[20].

Despite the development of various sensitization methods, the sensitizers still suffer from poor thickness and uniformity control especially for deposition on high aspect-ratio TiO_2 nanostructures. As the size of QDs is much larger than dye molecules, penetration of QDs into TiO_2 nanoarchitectures with a depth >10 μm is more difficult than the case in dye-sensitized solar cells[11]. Due to the quantum confinement effect and the limited charge diffusion length, the size of the QDs plays an important role in charge transfer process. The poor control in conventional deposition techniques usually leads to aggregation of QDs into large particles, thus causing high internal recombination loss.

Atomic layer deposition (ALD) is a thin film deposition technique that is based on self-limiting surface reactions by sequential exposure of the substrate to different gas phase precursors[21]. ALD provides precise thickness control at the angstrom or monolayer level and deposition on high aspect ratio nanostructures with

excellent step coverage. By employing ALD for QD sensitization, excellent infiltration and conformity could be achieved, and the size of QDs could be varied simply by tuning the number of ALD cycles. Recently Stacey et al showed the ALD CdS for solid state QDSSC[22]. However, there is a serious safety issue for such ALD CdS process, as the precursors of dimethyl cadmium (DMCd) and hydrogen sulfide (H_2S) are highly toxic.

Liquid-phase reaction via ion exchange has been developed as a method to fabricate semiconductor heteronanostructures[23,24]. The principle of ion exchange is based on the solubility of the material which allows only a critical selection of the target materials. Very recently ion exchange reaction has also been employed to fabricate nanowire p-n junctions for photovoltaics[25], as well as photosensitizer layers on ZnO nanowires for semiconductor-sensitized solar cells[26,27]. Due to its amphoteric property, ZnO is unstable for PEC in acidic or alkaline electrolyte solution, which is the bottleneck for practical applications. On the other hand, the amphipathicity of ZnO makes it an ideal template for nanofabrications[28].

In order to have the merit of ALD without the highly toxic source for the QD sensitization, in this work, ALD ZnO thin films were deposited on various TiO_2 nanostructures as the sacrificial templates to convert to short bandgap semiconductor sensitizers by ion exchange reaction (we call the whole process ALDIER). The thickness and the size of the sensitizer could be controlled by the thickness of the ZnO layer and the condition of ion exchange reaction. The reproducible photocurrent levels >15 mA/cm^2 is obtained using the TiO_2 inverse opals (TiIO), which is so far the highest among all nanostructure TiO_2-based PEC cell for hydrogen generation.

Results

Figure 1(a) illustrates the flowchart of the ALDIER based on the example of TiIO obtained by replicating a self-assembled multilayer polystyrene spheres[29,30]. However, the TiO_2 host structures for the 3-D homogeneous photosensitization can include a wide range of common types, for example, hydrothermal-grown nanorods, anodized nanotubes, and commercial P25 nanoparticles. In the first step, the host is coated with a layer of ZnO of tunable thicknesses using ALD. The second step is the ion exchange reaction. In this process the ALD ZnO layer serves as the sacrificial reactant which transforms first into ZnSe through anion exchange with the Se^{2-} precursor and then to the final CdSe via cation exchange with Cd^{2+} source[27]. The ion exchange reaction is based on the solubility product constant (K_{sp}) of the material. As the constant of ZnO ($K_{sp} = 6.8 \times 10^{-17}$) is much larger than ZnSe (3.6×10^{-26}), ZnO can be converted into ZnSe by anion exchange reaction with Se^{2-} anions. With the same principle, ZnSe can be further exchanged into CdSe (6.31×10^{-36}).

The sensitized TiIO is tested as the PEC photoanode in a three-electrode system for hydrogen generation. Figure 1(b) shows the diagram of the PEC cell where a piece of Pt foil was used as the cathode. H_2 gas bubbles are generated on the cathode through the water reduction reaction $2H^+ + 2e \rightarrow H_2$, whereas the holes are scavenged by the sulfide electrolyte. As CdSe has a wider light absorption range and better conduction band edge alignment with TiO_2 than ZnSe (see Fig. 1c), the photocurrent level of TiO_2/CdSe is much higher than TiO_2/ZnSe, as also reported in previous work[27]. Thus in this experiment we focus on CdSe photosensitizer on TiIO.

The composition transformation from ZnO to CdSe is confirmed using X-ray diffractometer (see Fig. 2a). The blue solid lines are the calculated XRD peaks for Anatase TiO_2 (PDF#21-1272), and the green dashed lines are the calculated XRD peaks for SnO_2 (PDF#41-1445). All the diffraction peaks of TiIO structure on FTO correlate well with the calculated positions. The diffraction peaks of ZnO (PDF#36-1451) appear only for the TiIO samples after the deposition of ZnO. After the first step anion exchange reaction, the ZnSe peaks (PDF#37-1463) can be detected while the ZnO peaks disappear, implying that the ALD ZnO layer is totally converted to ZnSe. After the complete exchange reaction, the peaks can be indexed to hexagonal CdSe (PDF#08-0459). The peak intensities of the CdSe

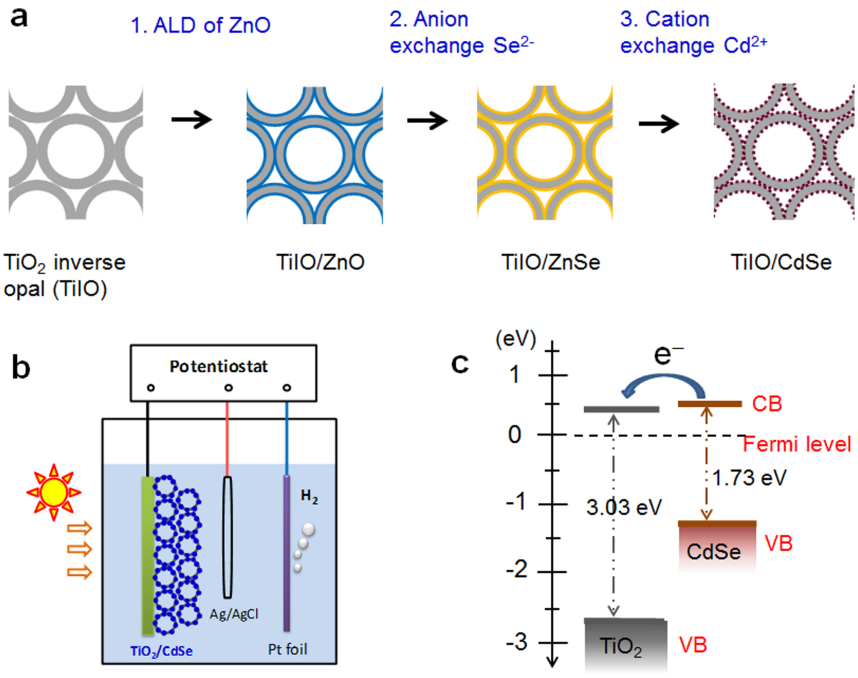

Figure 1 | Sensitization of TiO_2 inverse opals photoelectrochemical anode by ALDIER. (a) Schematics of the ALDIER process for uniform QD photosensitization of TiO_2 inverse opals (TiIO). Step 1: coating the TiIO with ALD ZnO layer. Step 2: anion exchange reaction converting the initial ZnO layer to ZnSe. Step 3: cation exchange reactions converting the intermediate ZnSe to CdSe. (b) Schematics of the photoelectrochemical cell: The as-prepared nanostructure serves as the anode, saturated Ag/AgCl as the reference electrode and the Pt foil as counter electrode for hydrogen evolution. (c) Electron energy levels of TiO_2 and CdSe. The photogenerated electrons within CdSe will be transferred to TiO_2, while the holes (not drawn) will be scavenged by the $Na_2SO_3 + Na_2S$ electrolyte solution. CB: conduction band. VB: valence band.

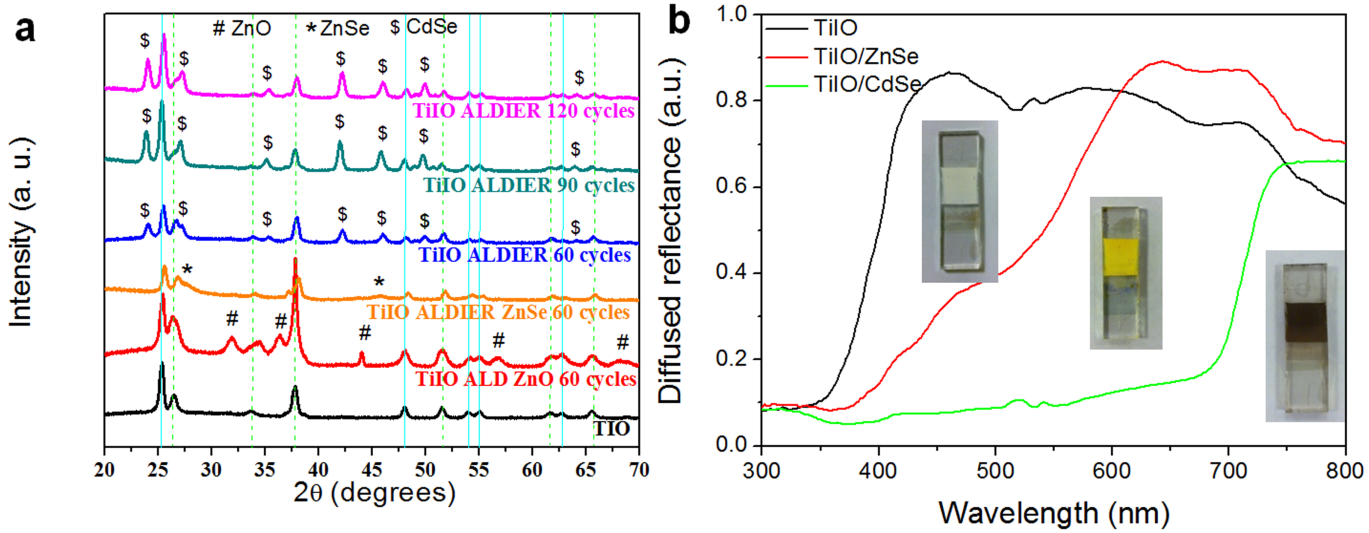

Figure 2 | Composition transformation. (a) XRD patterns of the pristine TiIO, and the derived structures after ALD and ion exchange reactions. The green dashed lines indicate the peaks of FTO, and the blue solid lines indicate peaks of anatase TiO_2. (b) UV-vis diffuse reflection spectra of three photoanode samples. TiIO: pure TiO_2 inverse opal. TiIO/ZnSe: ZnSe-coated TiIO after the anion exchange reaction. TiIO/CdSe: CdSe-coated TiIO after the cation exchange reaction. Insets are the photographs of the samples on FTO-coated glass.

increase from the 60-cycle sample to 120-cycle one, in accordance with the increased loading of CdSe.

UV-visible diffused reflection spectra are recorded to reveal the light harvesting capability of the pristine TiIO, ZnSe and CdSe sensitized TiIO photoanodes (results shown in Fig. 2b). The pristine TiIO can only absorb light with a wavelength below 400 nm. The absorption range broadens up to 550 nm after the exchange to ZnSe, and 700 nm after the final exchange into CdSe, consistent with their bandgaps. More diffuse reflection spectra for the samples at intermediate conversion stage are shown in Supplementary Fig. S1. The composition change after anion and cation exchange reactions and the light harvesting ability can also be revealed from the photographs of the samples in Fig. 2b inset. The samples with CdSe coating appear dark brown compared with the bright yellow coloured ZnSe and white pristine TiIOs.

Morphologies of the photoanodes prior to and after the ion exchange reactions with different ALD ZnO cycles are shown by SEM images in Fig. 3. The original TiIO surfaces are smooth. After ALDIER, the open surfaces are coated with a granular layer of CdSe. The SEM image in Fig. 3e provides an entire cross-sectional view of the structure with 60 ALD cycles (larger scale SEM images are provided in Supplementary Fig. S2). Clearly the ion exchange reactions proceed along the whole depth of 10 μm, owing to the effectiveness of ALD in creating conformal coatings on the surfaces of high aspect-ratio nanostructures. The morphology is further characterized using transmission electron microscopy (TEM). Figure 4a provides clear evidence of the attachment of nanoparticles on the available surfaces of TiO_2 pores. High-resolution TEM image in Fig. 4b shows that the particles are crystalline, and the lattice spacing can be indexed into (0-11) and (1-1-1) planes of hexagonal CdSe. Pure elements of Cd and Se are confirmed by the X-ray energy dispersion spectrum shown in Fig. 4c.

The PEC performance of the ALDIER photoanodes is investigated by conducting the current density vs potential (*J-V*) measurements under the dark and simulated sunlight illumination (AM 1.5) in the three-electrode cell configuration (Fig. 1b). First of all, all the electrodes are fabricated from 500 nm polystyrene spheres and have the same height of 10 μm. For ion exchange reaction, temperature is a critical parameter that affects the size and morphology of the resulting sensitizer layer. Hence the first step is to optimize the reaction temperature for CdSe exchange reaction while keeping ALD ZnO thickness the same (~10 nm by 60 ALD cycles). As shown in Supplementary Fig. S3, the electrode obtained from the reaction at 120°C exhibits the highest photocurrent level (15.7 mA/cm² at zero bias vs Ag/AgCl) compared to those from reactions at 90°C (4.6 mA/cm²) and 140°C (10.5 mA/cm²). Therefore, for the rest experiments, the reaction temperature is fixed at 120°C. Figure 5a presents the *J-V*

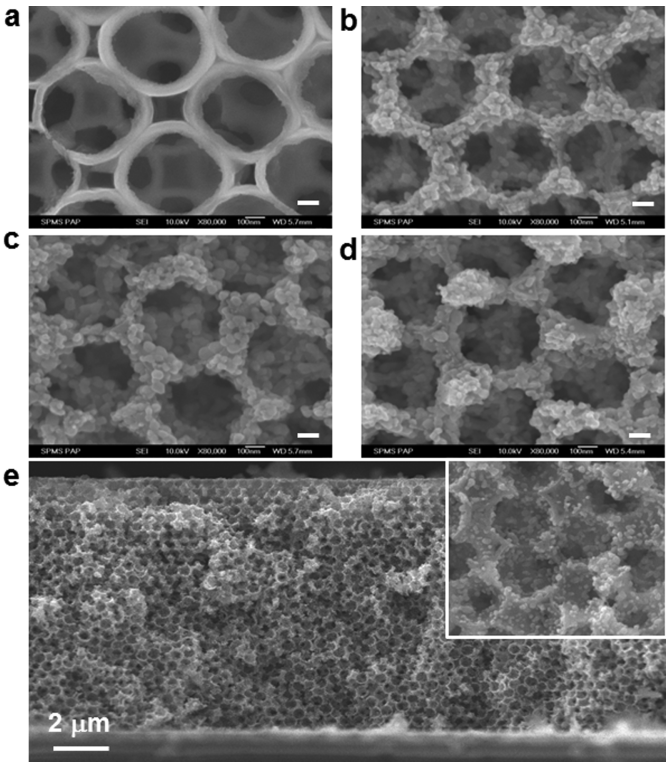

Figure 3 | SEM characterization. (a) Top view of the pristine TiO_2 inverse opal. (b-d) Top view images of the ALDIER samples, where the CdSe layers were converted from the ZnO starting layers obtained by using 60, 90, and 120 ALD cycles, respectively. Scale bars: 100 nm. (e) Side view of the entire cross section of the photoanode in (b) showing the uniform sensitization from top to the bottom. Inset: enlarged view of part of the cross section.

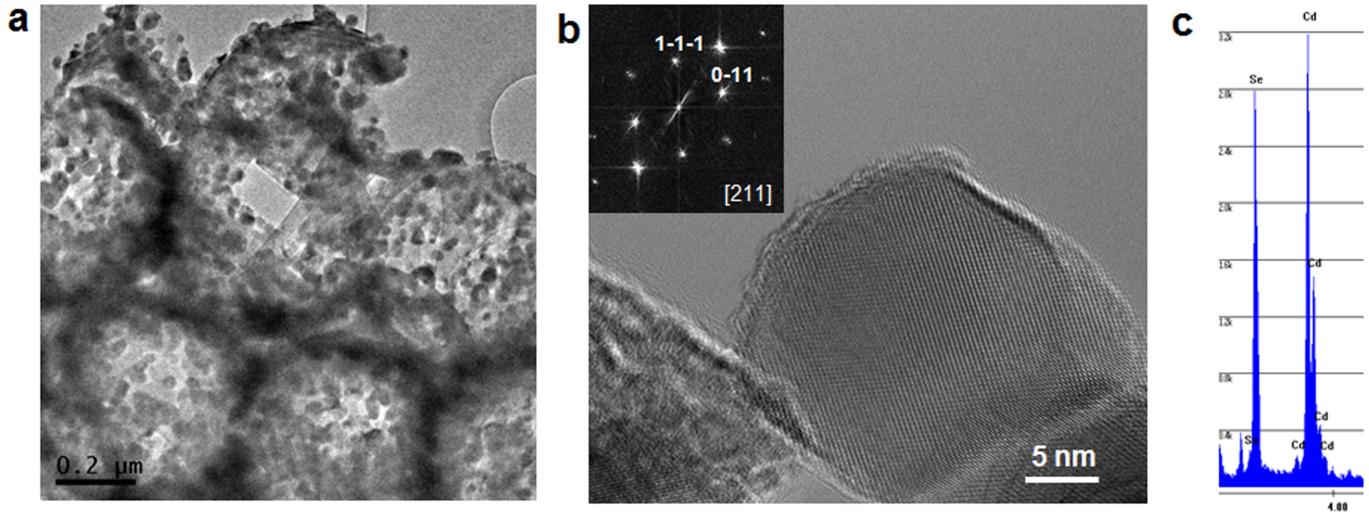

Figure 4 | TEM characterization. (a) Low-magnification TEM image of the CdSe nanoparticle-sensitized TiO_2 inverse opal. (b) Atomic-scale TEM image of one CdSe nanoparticle. Inset is the corresponding fast Fourier transformation pattern. (c) X-ray energy dispersion spectrum (EDS) recorded from the CdSe nanoparticle in (b).

curves of TiIO/CdSe anodes obtained from different ZnO ALD cycles. All the photoanodes present negligible dark currents while showing current densities above 10 mA/cm^2, upon illumination. This implies an efficient light harvesting by the sensitizers (see also IPCE below) and charge separation at the TiO_2 and CdSe interface rendered by the type-II band alignment (see Fig. 1c). All the samples show similar onset potentials (−1.0 V vs Ag/AgCl), as a result of similar surface flat bands. The photocurrents saturate

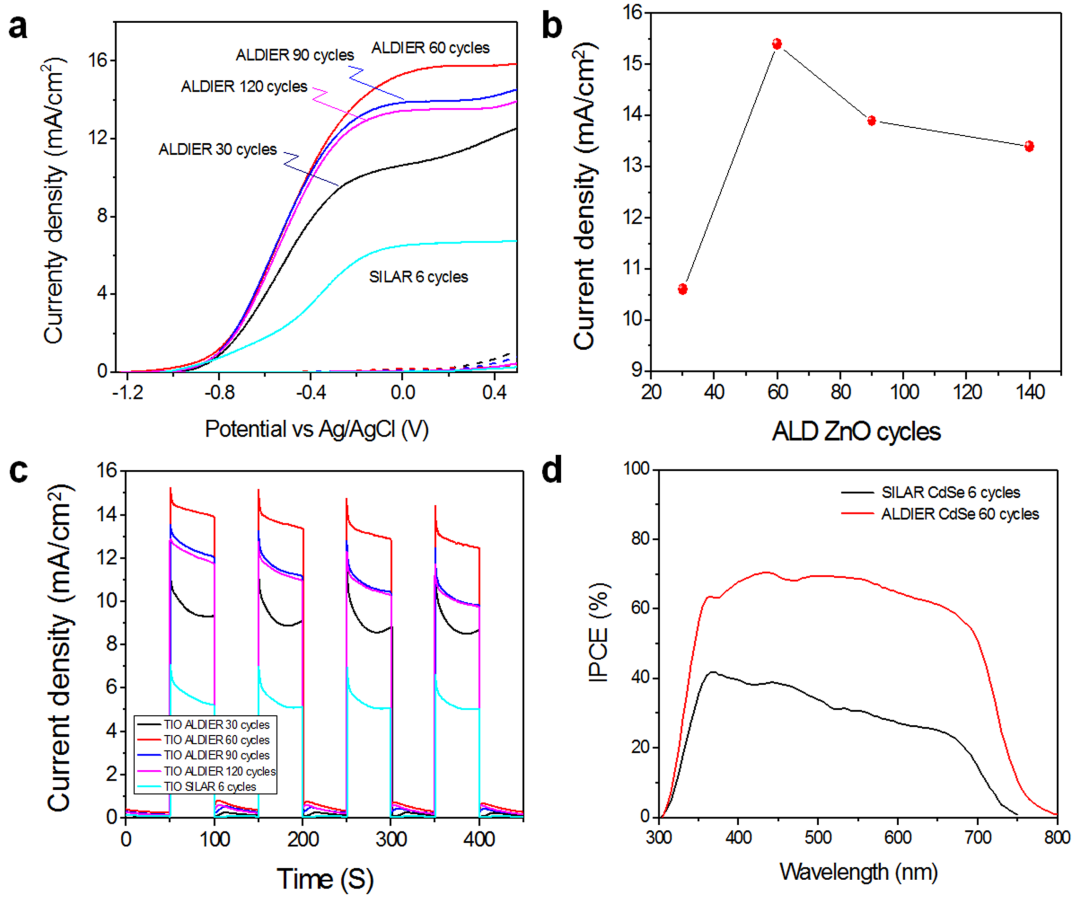

Figure 5 | Photoelectrochemical properties of the ALDIER TiO_2 inverse opal photoanodes. (a) Linear sweep voltammagrams (*J-V* curves) under dark condition and AM1.5 light illumination for samples by ALDIER technique with different ALD cycles, and one by 6 SILAR cycles. (b) Plot of the photocurrent density at zero bias in (a) versus the ALD ZnO cycle. (c) Photocurrent versus time tests (*J*−t curves) under chopped light illumination (light/dark cycles of 50 s) at a fixed bias of 0 V vs Ag/AgCl. (d) IPCE profile of the ALDIER photoanode with 60 ALD cycles. For comparison, the corresponding data of the optimized SILAR anode (6 cycles CdSe) are also shown.

with increasing bias voltage, indicating the good electrical conductivity of the TiIO/CdSe and the good contacts with the FTO.

We now discuss the effect of ALD ZnO thickness. Figure 5a-c show that the sample from 60 ALD cycles gives the highest photocurrents; further increment of the number of ALD cycles to 90 and 120 slightly bring the photocurrent down to ~13 mA/cm^2. The lowering of the current with higher ALD cycles might originate from adverse effects such as increased carrier recombination within the thicker CdSe layers. It is noted that a thicker ALD ZnO layer corresponds to a larger CdSe nanoparticle size. The photocurrent versus time ($J-t$) curves in Fig. 5c show that all the electrodes have good photoresponse and relatively good stability. For a comparison, a series of control samples of the same height are sensitized with CdSe via the SILAR method and measured under the same condition (see SEM images in Supplementary Fig. S4). Among samples with 3, 6, and 9 SILAR cycles, the highest photocurrent is ~6.5 mA/cm^2 obtained from the 6-cycle SILAR sample (also presented in Fig. 5a). The CdSe nanoparticles appear to have a lower coverage than that by ALDIER based on SEM inspection, which is consistent with the diffuse reflectance data, that is, the SILAR samples have a higher diffuse reflectance compared to that of ALDIER samples (see Supplementary Fig. S5 and Fig. S1). It is noteworthy that the photocurrent level obtained from our ALDIER electrodes is very high among nano TiO_2 photoanodes, even higher than the previously reported TiO_2 nanoparticle electrode with CdS and CdSe co-sensitization (14.9 mA/cm^2)[31].

While the voltammagram *J-V* curves show the overall PEC performance of the photoanode, the insight of the wavelength-dependent photocarrier generation can be obtained by studying the incident-photon-to-current conversion efficiency (IPCE), which allows the evaluation of the wavelength-dependent light harvesting efficiency. The IPCE profile from the 60-ALD cycle sample is shown in Fig. 5d. One can see that, within the test range of 300−800 nm wavelength, a strong and nearly constant photoresponse is observed in the visible region from 305 to 750 nm; the efficiency lies between 60−70% with a nearly flat profile. In contrast, the IPCE of the photoanode by SILAR sensitization is significantly lower, probably due to the aforementioned lower coverage of CdSe and the non-uniform sensitization, in correlation with its higher light reflectivity.

Discussion

The significant performance enhancement of ALDIER anodes compared with SILAR ones implies the superior quality of the sensitizer coating by this simple yet powerful ALD plus ion exchange technique, which results in an excellent penetration depth, uniform coverage and increased amount of loading of the sensitizers. As a result, both the light harvesting ability and the charge transfer would be enhanced. It is envisaged that the performance could be further improved by ZnS passivation as reported previously[32] or by doping of CdSe which is recently developed by the Kamat group[33].

To generalize this ALDIER technique to various nanostructures, same experiments are also conducted to TiO_2 nanorod arrays and nanoparticle films (see Supplementary Fig. S6 and S7). Shown in Fig. S6 are the results from the commercial P25 nanoparticle film. Clearly, one can also see the very low diffused reflectance and a high photocurrent level up to 12 mA/cm^2. The detailed study of the interface between CdSe and TiO_2 by the HRTEM and the inner charge transfer process by ultrafast optical spectroscopy is currently underway to provide a comprehensive physical understanding.

The demonstrated fabrication process can also readily result in CdS and PbSe if the anion exchange precursor is S^{2-} and the cation exchange precursor is Pb^{2+}, respectively. Due to the high conformity of the ALD ZnO layer[34], this simple two-step ALDIER process can be utilized for homogeneous coating of photoactive CdS, CdSe, PbS, or PbSe nanoparticles onto a wide range of complex and high-aspect-ratio substrates. Furthermore, as the thickness of the ZnO layer is precisely tunable by ALD cycles, the self-limiting ion exchange reaction will thus lead to different size and coverage of the final sensitizer nanoparticles.

To summarize, a new strategy based on ion exchange reaction using ALD ZnO layer as sacrificial template has been developed to coat TiO_2 nanostructures with a homogeneous layer of CdSe photosensitizer. With the optimized ion exchange reaction temperature and ALD ZnO thickness, the highest photocurrent for the TiIO/CdSe electrode reaches 15.7 mA/cm^2 at zero bias (versus Ag/AgCl), which is the highest value among TiO_2-based photoelectrochemical cells for hydrogen generation. Further in-depth insights of the enhancement mechanism will be studied in more details. This sensitization method can be generalized to other sensitizers like CdS, PbS, and PbSe. It is optimistic that such ALDIER method is ready to be extended to other TiO_2 nanostructures including anodized nanotubes, and to other electron transporting materials like SnO_2.

Methods

Fabrication of TiO_2 Inverse Opals. Carboxylate-modified, monodispersed polystyrene spheres of 500 nm diameter (Duke scientific corporation) were assembled onto the Fluorine-doped SnO_2 (FTO) coated glass substrates via a vertical deposition process at 90°C[29,30]. The self-assembled polystyrene spheres opals were then infiltrated with TiO_2 using a stop-flow-reactor ALD system at 70°C, for which titanium tetrachloride (99.99%, Sigma Aldrich) and H_2O were used as the Ti and O precursors, respectively. Finally, TiO_2 inverse opal structures were developed by burning the original polystyrene spheres in air at 450°C for 2 h, which also improved the crystallinity of the TiO_2. Last, reactive ion etching (RIE, NSC ES371) was used to cleave the top surface and open up the pores.

Preparation of TiO_2 particle film. TiO_2 nanoparticle films were deposited on the FTO by successive screen-printing using a TiO_2 paste consisting of Degussa P25 TiO_2 powder and an ethyl cellulose binder in α-terpinol[35]. The projected area of the TiO_2 layers was approximately 0.28 cm^2 (circles with 0.6 cm diameter). Then, the TiO_2 electrodes were gradually heated to 450°C where they were held for 15 min before being heated to 500°C for a further 30 min.

ALD ZnO layer and Ion Exchange Reactions. ZnO layers with different thickness were conformably deposited onto the TiIO as the sacrificial layers for the ion exchange reaction by ALD with the Diethyl zinc (DEZ, 99.99%, Sigma Aldrich) and H_2O as the Zn and O precursors, respectively. The ZnO coated TiIOs were then annealed in air at 450°C for 30 minutes to improve the crystallinity. TiIO/ZnSe core/shell structure was prepared by immersing the ZnO coated TiIO in a Se^{2-} ion solution (0.05 M, prepared by reacting 0.79 g Se powder with 0.8 g NaBH4 in 200 ml deionized water) and kept at 60°C for 5 hours in order to fully exchange the ZnO layer into ZnSe[27]. The samples were then washed with deionized water and absolute ethanol and fiwater dried in air. Due to the fact that Se^{2-} is vulnerable to oxygen, all the experiments containing Se^{2-} ions were done in glove box. The TiIO/ZnSe core/shell structures were then reacted with the 0.1 M $CdCl_2 \cdot 2.5H_2O$ aqueous solution at 90−140°C for 10 hours to replace Zn^{2+} by Cd^{2+} in the ZnSe shell. By controlling the reaction temperature, the composition of the TiIO/$Zn_xCd_{1-x}Se$ core/shell structure could be tuned. Finally, TIO/$Zn_xCd_{1-x}Se$ core/shell nanostructure was annealed in argon ambient at 400°C for 30 minutes to improve crystallinity.

Successive Ionic Layer Adsorption and Reaction (SILAR) of CdSe on TiIO. The SILAR process was modified from the previous reports[15,17]. In a typical procedure, the TiIO electrodes were immersed in a solution containing 0.05 M cadmium acetate dihydrate ($Cd(Ac)_2 \cdot 2H_2O$, Alfa Aesar, 98%) in ethanol for 1 min, to allow Cd^{2+} to adsorb onto the TiO_2 surface, and then rinsed with ethanol for 1 min to remove the excess Cd^{2+}. The electrodes were then dried for 2 min in an argon atmosphere. Subsequently, the dried electrodes were dipped in to a solution containing 0.05 M Se^{2-} for 1 min. The Se^{2-} solution was prepared by mixing selenium (Se, Sigma-Aldrich, 99.8%) and sodium borohydride (NaBH4, Sigma Aldrich, 99.8%) in water. The electrodes were then rinsed in ethanol for 1 min and dried again in an argon atmosphere for another 2 min. This procedure was repeated several times to get desired CdSe loading.

Materials Characterizations. The morphology and microstructure of the nanostructured films were examined using a JEOL JSM-7600F field emission scanning electron microscopy (FE-SEM), and a JEM 2100F transmission electron microscope (TEM). The X-ray diffraction (XRD) patterns were recorded by Shimadzu thin film XRD equipment using Cu Kα radiation. The diffuse reflection spectra were taken using Zolix Solar Cell QE/IPCE Measurement System equipped with an integrating sphere and a silicon diode detector.

Photoelectrochemical Characterizations. The PEC performance measurements were conducted in three electrodes configuration with the as prepared nanostructured photoanodes as working electrodes, Ag/AgCl in saturated KCl as a reference electrode and Pt foil as the counter electrode. 0.24 M Na_2S and 0.35 M

Na_2SO_3 mixed aqueous solution was used as the electrolyte. The current density vs potential ($J-V$) measurements were measured in both dark and illumination with a 150W Xe lamp (Science tech SS150) equipped with an AM1.5 G filter, calibrated with a standard Si solar cell to simulate AM1.5 illumination (100 mW/cm^2). Photocurrent versus time ($J-t$) tests were carried out by measuring the currents under chopped light illumination (light/dark cycles of 50 s) at a fixed bias of 0 V versus Ag/AgCl. The incident-photon-to-current conversion efficiency (IPCE) measurements were taken as a function of wavelength from 300 to 800 nm using a specially designed IPCE system for solar cells (Zolix Solar cell Scan100), with three electrodes configuration under zero bias versus Ag/AgCl. A 300 W Xe lamp equipped with gratings was used to generate a monochromatic beam. The incident light intensity was calibrated by a standard silicon photodiode.

1. Fujishima, A. & Honda, K. Electrochemical Photolysis of Water at a Semiconductor Electrode. *Nature* **238**, 37-38 (1972).
2. Chen, X. & Mao, S. S. Titanium dioxide nanomaterials: Synthesis, properties, modifications, and applications. *Chem. Rev.* **107**, 2891-2959 (2007).
3. Walter, M. G. *et al*. Solar Water Splitting Cells. *Chem. Rev.* **110**, 6446-6473 (2010).
4. Oregan, B. & Gratzel, M. A Low-Cost, High-Efficiency Solar-Cell Based on Dye-Sensitized Colloidal TiO2 Films. *Nature* **353**, 737-740 (1991).
5. Kamat, P. V. Quantum Dot Solar Cells. Semiconductor Nanocrystals as Light Harvesters. *J. Phys. Chem. C* **112**, 18737-18753 (2008).
6. Serpone, N. & Emeline, A. V. Semiconductor Photocatalysis — Past, Present, and Future Outlook. *J. Phys. Chem. Lett.* **3**, 673-677 (2012).
7. Serpone, N., Borgarello, E. & Gratzel, M. Visible-Light Induced Generation of Hydrogen from H2s in Mixed Semiconductor Dispersions - Improved Efficiency through Inter-Particle Electron-Transfer. *J. Chem. Soc., Chem. Commun.* 342-344 (1984).
8. Alivisatos, A. P. Semiconductor Clusters, Nanocrystals, and Quantum Dots. *Science* **271**, 933-937 (1996).
9. Peng, Z. A. & Peng, X. Formation of High-Quality CdTe, CdSe, and CdS Nanocrystals Using CdO as Precursor. *J. Am. Chem. Soc.* **123**, 183-184 (2000).
10. Robel, I., Subramanian, V., Kuno, M. & Kamat, P. V. Quantum Dot Solar Cells. Harvesting Light Energy with CdSe Nanocrystals Molecularly Linked to Mesoscopic TiO2 Films. *J. Am. Chem. Soc.* **128**, 2385-2393 (2006).
11. Mora-Sero, I. & Bisquert, J. Breakthroughs in the Development of Semiconductor-Sensitized Solar Cells. *J. Phys. Chem. Lett.* **1**, 3046-3052 (2010).
12. Watson, D. F. Linker-Assisted Assembly and Interfacial Electron-Transfer Reactivity of Quantum Dot-Substrate Architectures. *J. Phys. Chem. Lett.* **1**, 2299-2309 (2010).
13. Niitsoo, O. *et al*. Chemical bath deposited CdS/CdSe-sensitized porous TiO2 solar cells. *J. Photochem. Photobiol. A Chem.* **181**, 306-313 (2006).
14. Chang, C. H. & Lee, Y. L. Chemical bath deposition of CdS quantum dots onto mesoscopic TiO2 films for application in quantum-dot-sensitized solar cells. *Appl. Phys. Lett.* **91** (2007).
15. Lee, H. J., Bang, J., Park, J., Kim, S. & Park, S.-M. Multilayered Semiconductor (CdS/CdSe/ZnS)-Sensitized TiO2 Mesoporous Solar Cells: All Prepared by Successive Ionic Layer Adsorption and Reaction Processes. *Chem. Mater.* **22**, 5636-5643 (2010).
16. Lee, H. *et al*. Efficient CdSe Quantum Dot-Sensitized Solar Cells Prepared by an Improved Successive Ionic Layer Adsorption and Reaction Process. *Nano Lett.* **9**, 4221-4227 (2009).
17. Hossain, M. A., Jennings, J. R., Koh, Z. Y. & Wang, Q. Carrier Generation and Collection in CdS/CdSe-Sensitized SnO2 Solar Cells Exhibiting Unprecedented Photocurrent Densities. *ACS Nano* **5**, 3172-3181 (2011).
18. Banerjee, S., Mohapatra, S. K., Das, P. P. & Misra, M. Synthesis of Coupled Semiconductor by Filling 1D TiO2 Nanotubes with CdS. *Chem. Mater.* **20**, 6784-6791 (2008).
19. Lee, J.-C., Kim, T. G., Lee, W., Han, S.-H. & Sung, Y.-M. Growth of CdS Nanorod-Coated TiO2 Nanowires on Conductive Glass for Photovoltaic Applications. *Crystal Growth & Design* **9**, 4519-4523 (2009).
20. Islam, M. A., Xia, Y., Telesca, D. A., Steigerwald, M. L. & Herman, I. P. Controlled Electrophoretic Deposition of Smooth and Robust Films of CdSe Nanocrystals. *Chem. Mater.* **16**, 49-54 (2003).
21. George, S. M. Atomic Layer Deposition: An Overview. *Chem. Rev.* **110**, 111-131 (2010).
22. Brennan, T. P. *et al*. Atomic Layer Deposition of CdS Quantum Dots for Solid-State Quantum Dot Sensitized Solar Cells. *Adv. Energy Mater.* **1**, 1169-1175 (2011).
23. Son, D. H., Hughes, S. M., Yin, Y. & Paul Alivisatos, A. Cation Exchange Reactions in Ionic Nanocrystals. *Science* **306**, 1009-1012 (2004).
24. Robinson, R. D. *et al*. Spontaneous Superlattice Formation in Nanorods Through Partial Cation Exchange. *Science* **317**, 355-358 (2007).
25. Tang, J., Huo, Z., Brittman, S., Gao, H. & Yang, P. Solution-processed core-shell nanowires for efficient photovoltaic cells. *Nat. Nanotechnol.* **6**, 568-572 (2011).
26. Myung, Y. *et al*. Composition-Tuned ZnO−CdSSe Core−Shell Nanowire Arrays. *ACS Nano* **4**, 3789-3800 (2010).
27. Xu, J. *et al*. Arrays of ZnO/ZnxCd1–xSe Nanocables: Band Gap Engineering and Photovoltaic Applications. *Nano Lett.* **11**, 4138-4143 (2011).
28. Fan, H. J., Yang, Y. & Zacharias, M. ZnO-based ternary compound nanotubes and nanowires. *J. Mater. Chem.* **19**, 885-900 (2009).
29. Liu, L., Karuturi, S. K., Su, L. T. & Tok, A. I. Y. TiO2 inverse-opal electrode fabricated by atomic layer deposition for dye-sensitized solar cell applications. *Energy Environ. Sci.* **4**, 209-215 (2011).
30. Cheng, C. W. *et al*. Quantum-Dot-Sensitized TiO2 Inverse Opals for Photoelectrochemical Hydrogen Generation. *Small* **8**, 37-42 (2012).
31. Lee, Y.-L., Chi, C.-F. & Liau, S.-Y. CdS/CdSe Co-Sensitized TiO2 Photoelectrode for Efficient Hydrogen Generation in a Photoelectrochemical Cell. *Chem. Mater.* **22**, 922-927 (2009).
32. Mora-Seró, I. n. *et al*. Recombination in Quantum Dot Sensitized Solar Cells. *Acc. Chem. Res.* **42**, 1848-1857 (2009).
33. Santra, P. K. & Kamat, P. V. Mn-Doped Quantum Dot Sensitized Solar Cells: A Strategy to Boost Efficiency over 5%. *J. Am. Chem. Soc.* **134**, 2508-2511 (2012).
34. Yamada, A., Sang, B. & Konagai, M. Atomic layer deposition of ZnO transparent conducting oxides. *Appl. Surf. Sci.* **112**, 216-222 (1997).
35. Jennings, J. R., Liu, Y., Safari-Alamuti, F. & Wang, Q. Dependence of Dye-Sensitized Solar Cell Impedance on Photoelectrode Thickness. *J. Phys. Chem. C* **116**, 1556-1562 (2011).

Author contributions

JSL, SKK, and HJF designed the experiment, LJL fabricated the polystyrene inverse opals, LTS provided figure 4. JSL and SKK conducted the ALD and all characterizations. HJF and JSL wrote the manuscript text. AIYT provided part of the financial support. All authors reviewed the manuscript.

Additional information

Supplementary information accompanies this paper at http://www.nature.com/scientificreports

Competing financial interests: The authors declare no competing financial interests.

How to cite this article: Luo, J. *et al*. Homogeneous Photosensitization of Complex TiO_2 Nanostructures for Efficient Solar Energy Conversion. *Sci. Rep.* **2**, 451; DOI:10.1038/srep00451 (2012).